Journal of Neonatal Surgery
ISSN(Online): 2226-0439
Vol. 14, Issue 1s (2025)
https://www.jneonatalsurg.com

OPEN ACCESS

AElm-XGB: Hybrid Machine Learning Based Automated Classification of Oral Cancer by Effective Segmentation

Smita Baghel[1], Dr. Anupam Shukla[2]

[1]Phd Scholar, Indian Institute of Information Technology, Pune.

[2]Director, SVNIT, Surat, Tanmoy Hazra, Assistant Professor, (Grade-I), SVNIT, Surat.

Cite this paper as: Smita Baghel, Dr. Anupam Shukla, (2025) AElm-XGB: Hybrid Machine Learning Based Automated Classification of Oral Cancer by Effective Segmentation. *Journal of Neonatal Surgery*, 14 (1s), 1174-1192.

ABSTRACT

Medical professionals benefit from early cancer disease detection because it shortens the time between diagnosis and treatment. In small towns and rural areas where people are less aware of the risks associated with tobacco and cigarette use, OC may have a high mortality rate due to its severe effects. The technique is insufficient for detecting OC disease in its early stages. Since people only live for five years on average after being diagnosed with OC disease, its detection may be possible at a later stage. By overcoming certain demerits of existing works, the proposed research work presents a novel machine learning (ML) based methodology for accurate diagnosis of oral cancer. At first, the input images are collected and pre-processed using the Quadruple Clipped Enhanced Histogram equalization (QCeHE) for enhancing the image contrast and Adaptive Prewitt and Laplacian of Gaussian filtering (ApLG) for noise removal. After the pre-processing step, hybrid segmentation is done on the basis of Expanded gate attention U-Net model (ExpG-UNet) method. Here the original images will be trained with that of generated ground truth images to obtain the segmented output. The features are extracted based on Integration of discrete wavelet transform, principle component analysis and gray level co-occurrence matrix (DWT-PCA-GLCM) method and extracted features are fused together. The features are provided to the machine learning method called Advanced Hybrid Extreme Learning Machine and Extreme Gradient Boosting (AElm-XGB) to classify the oral cancer effectively. The losses can be optimized by using African Vulture Optimization (AVO).The proposed model can accurately detect the oral cancer effectively. In the evaluation, the proposed model achieved 98.67 % accuracy. Diabetes mellitus, particularly type 2 diabetes, is a growing global health issue, often exacerbated by insulin resistance, metabolic disturbances, and inflammatory responses. Emodin, a natural anthraquinone derivative, has been widely recognized for its pharmacological properties, including its antidiabetic potential. This study investigates the therapeutic efficacy of emodin in ameliorating Type 2 diabetes in Wistar albino rats induced by streptozotocin (STZ). Male rats were divided into healthy, diabetic, and treatment groups, with diabetic groups receiving emodin (40 mg/kg body weight/day, orally) or metformin for 45 days. Diabetes induction was confirmed by elevated blood glucose levels, altered lipid profiles, and reduced insulin sensitivity. Emodin administration significantly reduced fasting blood glucose levels and improved glucose tolerance, comparable to metformin treatment. Biochemical analyses revealed that emodin restored the lipid profile, enhanced antioxidant enzyme activity, and suppressed oxidative stress markers in diabetic rats. The study revealed that emodin exhibited antidiabetic effects by regulating glucose metabolism, enhancing insulin sensitivity, and reducing oxidative stress. Data expressed as mean ± SEM showed significant differences ($p<0.05$) among control, diabetic control, emodin-treated, and metformin-treated groups. Emodin treatment notably improved glucose metabolism and outperformed metformin in reducing insulin resistance. These findings highlight emodin's potential as a therapeutic agent for Type 2 diabetes by targeting insulin resistance, inflammation, and metabolic dysregulation. Emodin holds promise for managing diabetes and its complications effectively.

Keywords: *Quadruple Histogram, Prewitt and Laplacian filter, African Vulture Optimization, U-Net model, Extreme Learning Machine, XG Boost.*

1. INTRODUCTION

Globally, oral cancer (OC) has become a major problem for public health. According to the literature, between 1990 and 2017, this disease's global incidence, death, and disability-adjusted life years increased by almost 1.0-fold. According to GLOBOCAN's forecasts of morbidity and prevalence, and there will be 377,713 new cases and 177,757 fatalities from lip and oral cavity cancer in 2020 [1]. The majority (more than 85%) of cases of OC are squamous cell carcinoma of the oral cavity. Even though early diagnosis of OC is crucial, the majority of patients are diagnosed when the disease is already

advanced, which leaves them with a poor prognosis. Therapy choosing based on the clinical appearance of the illness is unsatisfactory because the clinical appearance of OC is to identify the dysplastic state, analysis, or degree [2]. To maximize survival and quality of life after treatment, OC must be detected early [3].

Many image processing systems are frequently used to detect OC earlier, which increases cancer survival rates and improves treatment effectiveness. By examining magnetic resonance imaging (MRI) scans, X-rays, and computed tomography (CT) images, medical imaging techniques, computer-aided detection, and diagnosis, have the potential to change how cancer is treated because cancer can now be detected in an earlier stage [4, 5]. In oncology research, machine learning (ML) algorithms that automate the construction of analytical models have been used to enhance prediction and make more accurate projections of clinical outcome [6]. Their popularity is based on a presumption that they have the capacity to sequentially identify patterns, collect data, engage in automated training based on data input, particularly complex non-homogenous data, and eventually produce clinical predictions with little to no human involvement [7].

The three factors that are crucial for an early diagnosis and prognosis were found to be advantageous in the ML approach. These are more accurate cancer susceptibility, recurrence, and overall survival projections that increase by effectively managing patients' conditions [8]. There are three types of preventive measures: primary, secondary, and tertiary. Increased public awareness of risk factors and public behavior change are the main objectives of primary preventive measures. Through screening methods, secondary prevention aims to find malignant lesions early. The goal of tertiary prevention is to protect patients from OC [9]. Emerging demand in using phytochemical components to treat or prevent cancer. These phytochemicals are excellent chemo preventive agents because they have low to no toxicity toward healthy tissues [10].

Therefore, educating people about limiting behavioral risk factors, discouraging tobacco use and addiction, and limiting alcohol consumption constitute prevention of OC. The early detection and treatment of oral pre-malignancies and early-stage cancers constitute secondary prevention [11]. OC is frequently found using a variety of conventional clinical techniques, including histopathological examination and physical, spectroscopic, biopsy, staining, and radiological techniques, etc. Early cancer detection is crucial for preventing the patient from suffering psychological additional, physical, and financial losses. Early diagnosis allows for timely and effective treatment to begin, which can increase survival rates by up to 90% [12, 13].

Chemotherapy, radiation therapy, and surgery are currently the three main cancer treatment modalities. Each of these approaches has drawbacks, such as harm to the nerves, blood vessels, and bone in the oral and maxillofacial region, as well as a number of other problems with quality of life. Therefore, there is a pressing need for more focused, minimally invasive, and extremely effective methods of treating OC. One of the existing methods for identifying cancer and categorizing its type is medical imaging. Invasive procedures, skin removal, and free flap introduction in the cancer area are the drawbacks of surgical cancer resection. Imaging methods are now more effective for treating cancer as a result [14, 15].

1.1 Motivation and problem statement

The primary factor behind this cancer study is concern for human health. Due to its severe effects, OC may result in a high mortality rate, particularly in small towns and rural areas where residents are less aware of the dangers of tobacco and cigarette use. The method for identifying OC disease in its early stages is insufficient. As a result, its detection may be possible at a later stage, and as a result, after OC disease diagnosis, people only live for five years on average. Early disease detection is possible through the application of efficient ML techniques, segmentation and hybrid feature extraction approach. As a result of the disease dataset's erratic and irrelevant data values, the accuracy of the predicted outcome is insufficient. Pre-processing techniques allow for the removal of noisy data and contrast enhancement, which increases accuracy percentage and makes it possible to predict disease based on early stage symptoms. By considering the above limitations of various existing works, a novel technique has been proposed to detect the OC effectively. The main contribution of this study is given as follows.

- To present pre-processing approach using Quadruple Clipped Enhanced Histogram equalization (QCeHE) for enhance the image contrast and Adaptive Prewitt and Laplacian of Gaussian filtering (ApLG) for noise removal.
- To perform hybrid segmentation method called, Expanded gate attention U-Net model (ExpG-UNet) that can effectively segment the area of oral cancer and it takes less time to segment.
- To extract the features using Integration of discrete wavelet transform, principle component analysis and gray level co-occurrence matrix (DWT-PCA-GLCM) method based feature extraction approach for extract the features efficiently.
- To classify the extracted features using Advanced Hybrid Extreme Learning Machine and Extreme Gradient Boosting (AElm-XGB) model for better detection of oral cancer.

The paper is organized from the introduction of oral cancer as given in the section. The existing models used for oral cancer is described in Section 2. The proposed model detail is provided in the section 3 and the results are given in Section 4. The conclusion and future scope of the proposed model is given in the Section 5.

2. RELATED WORKS

Kumari et al. [16] suggested a machine learning (ML)-based method and multistage feature extraction for OC detection in various mouth locations using regular oral images. Principal component analysis (PCA), gray level co-occurrence matrix (GLCM), and histogram-oriented gradients (hog) were used for pre-processing and feature extraction, respectively. The tests made use of 131 images, 44 of which were normal and 87 of which were aberrant, from a real human oral imaging dataset. On test images, the Support vector machine's (SVM) classification accuracy was an impressive 80.95%.

Jeyaraj et al. [17] recommended partitioned deep Convolution Neural Network (CNN) for classifying and labeling by labeling the region of interest in multidimensional hyperspectral image has two partitioned layers. By assessing classification accuracy, the partitioned deep CNN's performance was confirmed. For task classification of malignant cancer with benign and for task classification of with normal tissue accuracy of 94.5% for 500 training patterns was obtained, we obtained classification accuracy of 91.4% with sensitivity 0.94 and a specificity of 0.91 for 100 image data sets.

Jubair et al. [18] presented light weight deep convolutional neural network (CNN) for binary classification of oral lesions into benign and malignant or potentially malignant lesions. For the diagnosis of OC, low-cost embedded vision devices with constrained memory and processing power may be built effectively using deep CNN. The light weight deep CNN model achieved an accuracy of 85.0%, a specificity of 84.5%, sensitivity of 86.7% and an AUC of 0.928.

Panigrahi et al. [19] offered capsule network that is used to classify the OC. The capsule network is more resistant to rotation and affine transformation of the augmented oral dataset thanks to dynamic routing and routing by agreement. This network is suitable for early analysis of OC histopathological images because it can handle pose, view, and orientation. Cross-validation results show that the suggested methodology can accurately classify histopathological images of oral squamous cell carcinoma (OSCC) with 97.35% precision, 96.92% specificity, and 97.78% sensitivity.

Huang et al. [20] progressed convolutional neural network (CNN)/ ISSA that is used to classify accurate diagnosis of OC. Gamma correction, noise reduction, and data augmentation are the first three pre-processing methods used to improve the quality and quantity of the raw images in order to generate enough data for convolutional neural network training. ISSA (an improved version of the squirrel search algorithm) then selects the network weights optimally to provide greater accuracy. Analysis of various existing works that are related to the OC classification presented in Table 1.

Table 1: Analysis of various existing works that are related to the OC classification

Author & Reference	Techniques used	Objective	Limitation	Performance
Kumari et al. [16]	ML	To classify the OC with high accuracy.	Dataset: small in size. Poor resolution images.	Accuracy of 80.95%.
Jeyaraj et al. [17]	Partitioned deep Convolution Neural Network (CNN)	To classify the malignant and benign OC cancer effectively.	Low accuracy.	Accuracy of 94.5%, Sensitivity of 0.94%, and Specificity of 0.91%.
Jubair et al. [18]	Light weight deep convolutional neural network (CNN)	The Binary classification of oral lesions into benign and malignant.	The datasets images are made for clinical only.	Accuracy of 85.0%, Specificity of 84.5%, Sensitivity of 86.7%, and AUC of 0.928.
Panigrahi et al. [19]	Capsule network	To analyse the OC at an early stage effectively.	No spatial relationship.	97.35% of precision, 96.92% specificity, and 97.78% sensitivity.
Huang et al. [20]	CNN/ISSA	To provide an appropriate diagnosis of OC in the early stage.	Low image quality.	97.33% of accuracy, 92.66% of precision, 89.37% of F1-score, and 87.34% of sensitivity.

From the review of existing models, various challenges of oral cancer detection is revealed. The major challenges faced in the reviews were generalizability issue due to limited samples of data. Some models have Poor resolution images which degrade the performance in the classification. The datasets images are made for clinical data results in weak performance and leads to adoptability issues. The spatial relationship among the data and features are inappropriate which makes an issue in true positive values that decrease the performance. Hence, the proposed model is implemented to overcome the challenges in the existing models.

3. PROPOSED METHODOLOGY

This work proposes an innovative approach by integrating Quadruple Clipped Enhanced Histogram equalization for pre-processing mechanism. Further the Adaptive Prewitt and Laplacian of Gaussian filtering is used for effective noise reduction because noise can degrade the quality and clarity of an image, and affect its usefulness for target analysis. The pre-processed results are fed into an expanded gate attention U-Net model for efficient hybrid segmentation, which partitions the image into multiple image segments. Then the output of the segmented images are obtained by training the original images with generated ground truth images. The segmented images undergoes feature extraction with the combination of discrete wavelet transform, principle component analysis and gray level co-occurrence matrix, which are fused together accordingly. Next these extracted features are provided for Advanced Hybrid Extreme Learning Machine and Extreme Gradient Boosting for effective classification. Finally a meta-heuristic algorithm is proposed for loss optimization. Hence, the proposed model detects the oral cancer regions efficiently. The work flow of the proposed approach is depicted in Figure 1.

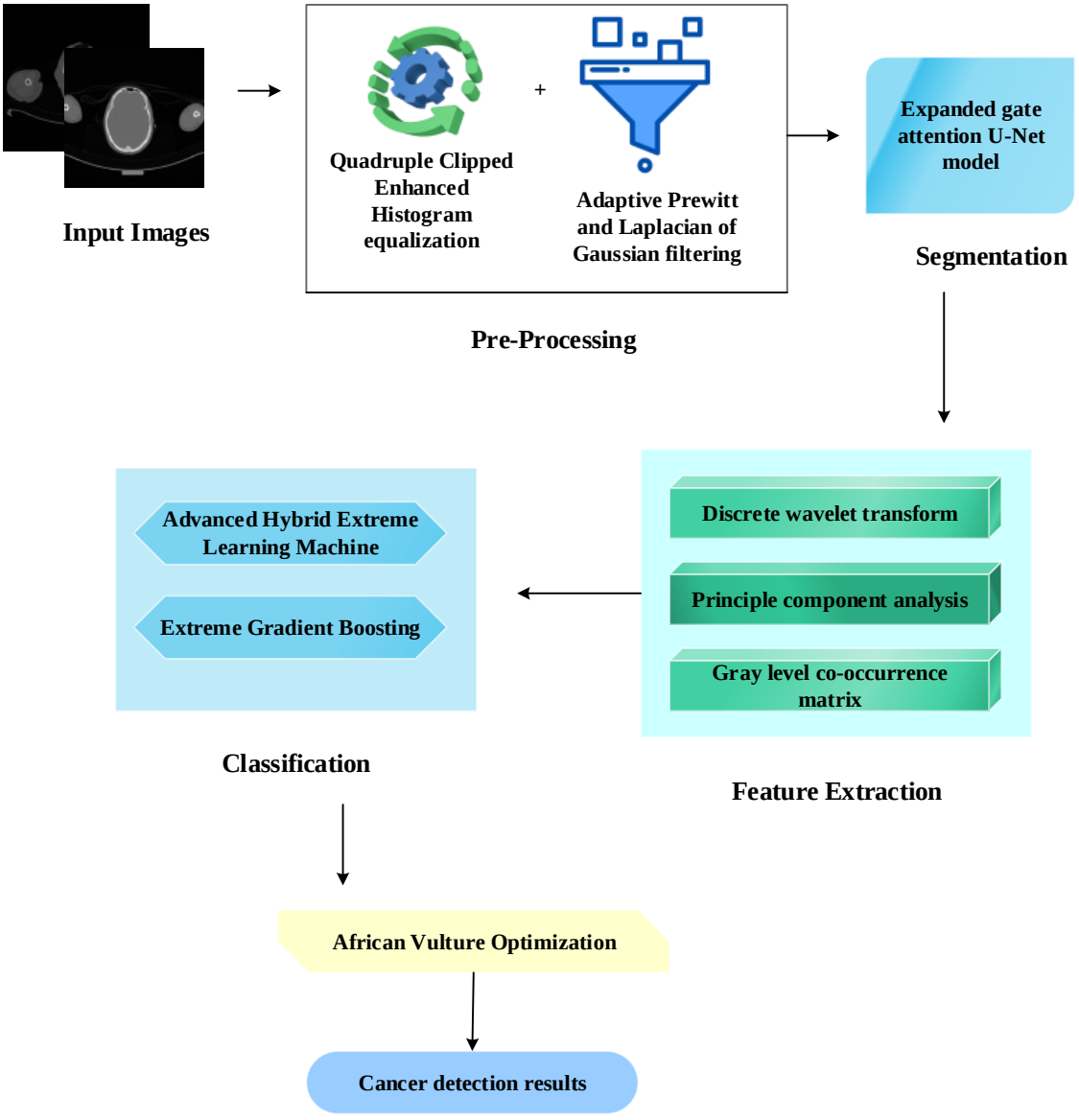

Figure 1: Proposed Model Work Flow

The proposed workflow begins with data pre-processing of input images by QCeHE and ApLG filters are used for noise removal of the image. Then the segmentation of images are done by using, ExpG-U Net model. Further the feature extraction is determined by DWT-PCA-GLCM model. These fused extraction features are fed for the proposed model AELm-XGB for effective classification of images. Next the loss can be optimized by using AVO. Finally, the oral cancer regions are detected by the proposed model.

3.1 Pre-processing

Image pre-processing is a set of techniques employed to enhance the quality and extract relevant information from images before they are further analyzed and processed by computer vision or other machine learning algorithms. It involves a set of operations that aim to correct, filter, normalize, or enhances the images in order to improve their suitability for subsequent analysis. It also helps in identifying incorrect, incomplete, irrelevant parts of the data and then modifying, replacing, or deleting those unwanted data from the dataset. Hence, pre-processing removes the noisy data, containing errors, outliers, missing values, or inconsistencies, which can affect the quality and reliability of the target exploration. The work flow diagram of pre-processing is shown in Figure 2.

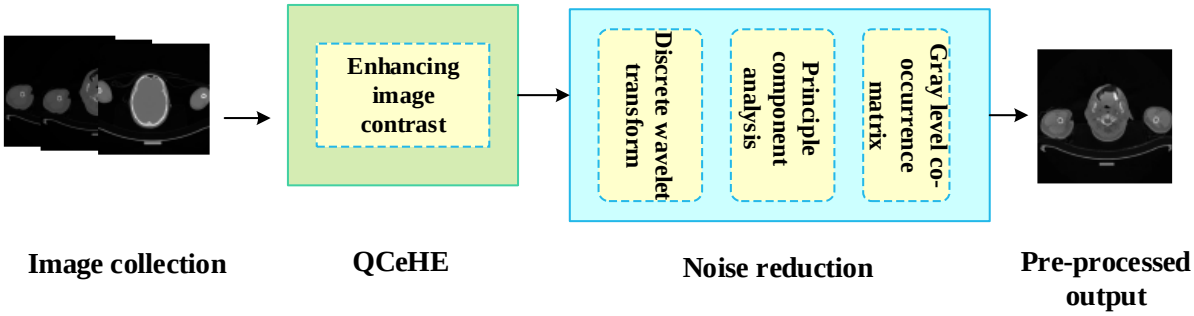

Figure 2: Workflow of pre-processing

Figure 2 describes that the input images are fed into a pre-processing model named, QCeHE for detecting or removing corrupt and inaccurate images from a dataset. Therefore, QCeHE enhances the image contrast by sharpening the image. Further the noise elimination is done by the fusion of three models namely, DWT-PCA-GLCM for efficient removal of unwanted or random variations in pixel values of an image. Finally, the pre-processed output is generated for segmentation.

3.1.1 Quadruple Clipped Enhanced Histogram equalization

Quadruple Clipped Enhanced Histogram Equalization [21] is a computer image processing technique used to improve contrast in images. QCeHE undertakes this by effectively spreading out the most frequent intensity values, by stretching out the intensity range of the image. This method usually increases the global contrast of images, in which its usable data is represented by close contrast values. This allows the areas of lower local contrast to gain a higher contrast. The Proposed QCeHE model underlines to improve the image quality, minimizing information loss, preserving the brightness and optimizing the over enhancement rate without affecting the structure and feature of the low exposure images. Then the exposure values are evaluated by using equation (1).

$$EX_{pos} = \frac{1}{G_{level}} \frac{\sum_{f=1}^{G_{level}} gi(f)f}{\sum_{f=1}^{G_{level}} gi(f)} \quad (1)$$

Where, the variable EX_{pos} represents the exposure value, $gi(f)$ is the histogram function and the maximum gray level is represented by the"G_{level}".

The output of the histogram images is completely changed as compare to input histogram by amplifying noise. So, histogram of the input image is separated into four sub-histograms using exposure threshold of the image and mean of each sub-histogram. The traditional histogram equalization algorithm enhances the contrast of an image by redistributing its pixel values. The main process of the algorithm involves calculating the probability density function (PDF) and cumulative distribution function (CDF) of the histogram and then using these values to generate a pixel mapping table, the conversion formula of histogram equalization. Hence, the calculation of PDF and CDF is determined by the equation (2) & (3).

$$PROB_{denf}(f) = \frac{m_f}{M} \quad (2)$$

$$CUMU_{drif}(f) = \sum_{p=first}^{f} PROB_{denf}(p) \quad (3)$$

Where, "f" is the gray level, "m_f" is the number of pixels corresponding to the "f" gray level in the image histogram, and "M" is the total number of pixels in the interval. Therefore, the transformation formula for enhanced histogram equalization

is depicted in equation (4).

$$K(f) = first + CUMU_{drif}(f) \times (last - first) \quad (4)$$

In the above equation, the "$last$" represents the final value of the mapping interval, the "$first$" represents the starting value, and "$last - first$" represents the mapping interval length.

When the traditional segmentation algorithm based on exposure value encounters a narrow distribution range in the histogram, the calculated exposure threshold may fall out. Hence the optimized histogram distribution range is determined in equation (5).

$$\begin{cases} Small = min(m_f \geq n), f\epsilon[0, G_{level} - 1] \\ Big = max(m_f \geq n), f\epsilon[0, G_{level} - 1] \end{cases} \quad (5)$$

The above equation that depicts the intervals formed by the minimum and maximum value of the statistics in the histogram, which is not less than"n". Therefore the new exposure value and the split point can be calculated by using the equation (6) & (7).

$$EX_{pos} = \frac{\sum_{f=Small}^{Big} m_f(f-Small+n)}{(Big-Small)\times\sum_{f=Small}^{Big} m_f} \quad (6)$$

$$Z_x = Small + (1 - EX_{pos}) \times (Big - Small) \quad (7)$$

Where, "Z_x" represents the exposure threshold. After segmenting the histogram into two sub-histograms, the mean of the two sub-histograms is determined by the equation (8) & (9).

$$Z_1 = \sum_{f=Small}^{f=Z_x-1} Q_{dl}(f) \times f \quad (8)$$

$$Z_2 = \sum_{f=Z_x}^{f=Big-1} Q_{du}(f) \times f \quad (9)$$

Where, Z_1 and Z_2 represent the means of the two sub-histograms respectively, $Q_{dl}(f)$ and $Q_{du}(f)$ represent the PDFs of the two sub-histograms, respectively. The evaluation of $Q_{dl}(f)$ and $Q_{du}(f)$ is depicted in equation (10) & (11).

$$Q_{dl}(f) = \frac{gi(f)}{m_t}, \quad for\ 0 \leq f \leq Z_x - 1 \quad (10)$$

$$Q_{du}(f) = \frac{gi(f)}{m_v}, \quad for\ Z_x \leq f \leq G_{level} - 1 \quad (11)$$

Therefore, for four sub-images having gray level ranges from 0 to $Z_1, Z_1 + 1\ to\ Z_x, Z_x + 1\ to\ Z_2, Z_2 + 1\ to\ G_{level} - 1$, respectively. Now, the PDF of each sub-histograms are calculated by using the equation (12) to (15).

$$Q_{dl1}(f) = \frac{gi(f)}{m_{t1}}, \quad for\ 0 \leq f \leq Z_1 \quad (12)$$

$$Q_{dl2}(f) = \frac{gi(f)}{m_{t2}}, \quad for\ Z_1 \leq f \leq Z_x \quad (13)$$

$$Q_{du1}(f) = \frac{gi(f)}{m_{v1}}, \quad for\ Z_x \leq f \leq Z_2 \quad (14)$$

$$Q_{du2}(f) = \frac{gi(f)}{m_{v2}}, \quad for\ Z_2 + 1 \leq f \leq G_{level} - 1 \quad (15)$$

Here,m_{t1}, m_{t2}, m_{v1} and m_{v2} are the number of pixels of respected sub-images. Hence, the QCeHE plays an important role in adjusting the contrast of the image by modifying the intensity distribution of the histogram.

3.1.2 Image Filtering

Image filtering refers to changing the appearance of an image by altering the colours of the pixels. Increasing the contrast as well as adding a variety of special effects to images and reducing noise are some of the results of applying filters. Here, the proposed model utilizes two different kinds of hybrid filters for effective enhancement of the image.

3.1.2.1 Adaptive Prewitt filtering

The Prewitt filter [22] is used for detecting vertical and horizontal edges in images. This filter uses two 3×3 kernels. The two kernels are shown in equation (16) & (17).

$$GRAY_{val1} = \begin{bmatrix} +1 & 0 & -1 \\ +1 & 0 & -1 \\ +1 & 0 & -1 \end{bmatrix} * X(z, w) \quad (16)$$

$$GRAY_{val1} = \begin{bmatrix} +1 & +1 & +1 \\ 0 & 0 & 0 \\ -1 & -1 & -1 \end{bmatrix} * X(z,w) \quad (17)$$

Here, "X" is the image source and " $*$ " is the 2D convolution operation.

3.1.2.2 Laplacian of Gaussian filtering

LoG filtering [23] targets to reduce the noise level in the image. This filter consists of two steps, firstly smooth image by using a Gaussian filter, then applying the Laplacian to find edges, which can be calculated by the equation (18).

$$LAP_{GAU_{filter}}(x,e) = -\frac{1}{\rho\tau^4}\left[1 - \frac{x^2+e^2}{2\tau^2}\right] s^{\frac{x^2+e^2}{2\tau^2}} \quad (18)$$

Here, "(x,e)" is the spatial coordinates of the image pixel and "τ" is the kernel size of the Gaussian filter.

3.2 Segmentation

Image segmentation is the process of partitioning an image into multiple image segments. Medical image segmentation targets to make anatomical or pathological structure changes in more clear images and it often plays a key role in computer-aided diagnosis and smart medicine due to its great improvement in diagnostic efficiency and accuracy. In order to achieve pixel classification of an image, an encoder-decoder or attention U-Net models can be proposed for effective segmentation of an image.

3.2.1 Expanded gate attention U-Net model

Attention mechanisms play a crucial role in human perception. Attention mechanisms allow humans to selectively focus on key information while ignoring other irrelevant information. Hence in gate attention module, U-Net model [24] can accelerate the learning process, extract more critical and discriminative features for the target task, which further enhances the robustness of the network model, and be more adaptable to small training datasets. The architecture of Expanded gate attention U-Net model is depicted in figure 3.

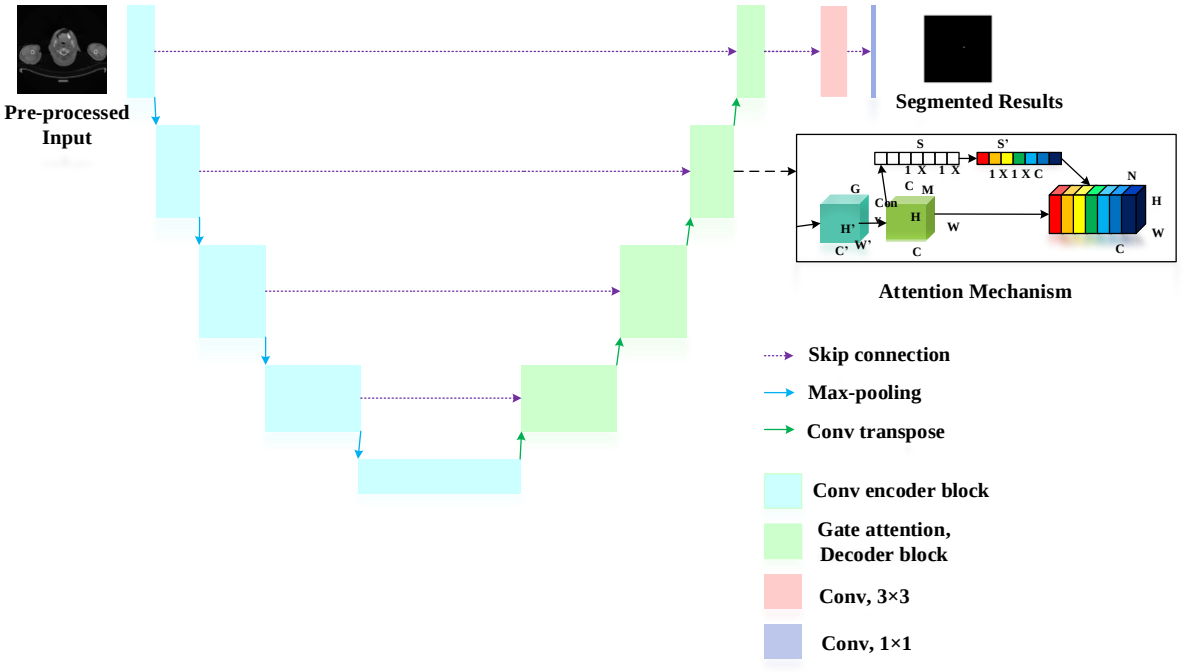

Figure 3: Architecture of Expanded gate attention U-Net model

Figure 3 illustrates, ExpG-UNet with a network structure similar to that of a U-shaped encoder decoder. Each step of the encoder and decoder consists of a structured convolution block and a gate attention decoder block, respectively. Each convolutional block consists of a convolutional layer (Conv Block), normalization layer etc. In the encoder path, the network doubles the number of feature channels with each down-sampling step. This corresponds to an up-sampling of the 2 × 2 transpose convolution, which splits the number of feature channels in the decoder path. The encoder and decoder are connected by skips between the feature maps of the corresponding layers before a structured gate attention decoder block is performed. Cancer lesion output segmentation maps are generated at the last layer, after 1 × 1 convolution functions.

3.2.1.1 Gate attention mechanism

The model's gate attention mechanism highlights salient features useful for a specific task while suppressing irrelevant regions in an input image. The gate attention selects spatial regions by analyzing the contextual information and activation provided by the gating signal h_{sig} collected from coarser scales. The input features $(a \cdot t)$ are scaled according to the attention coefficients "δ" of the resampled grids, which are completed using trilinear interpolation. The attention factor $\delta i \in [0,1]$is used to identify significant image areas and to determine the focal area. The output of gate attention is the multiplication of the elements of the input feature mapping and the attention factor, as $\hat{a}\, ti, d = a\, ti, c \cdot \delta\, ti$. In the default setting, a single scalar focus value is calculated for each pixel vector $a\, ti \in EKt$, where "K" corresponds to the number of feature maps in layer "t". A gating vector $h_{gate}i \in EKh$, which is used for each pixel to determine focus regions. Moreover, the additive attention is formulated in the equation (19) & (20).

$$p_{ation}^{t} = \chi^{L}\left(\delta_1\left(Y_a^L a_i^t + Y_{h_{gate}}^L h_{gate_i} + r_{h_{gate}}\right)\right) + r_{\chi} \qquad (19)$$

$$\delta_i^t = \delta_2\left(p_{ation}^t\left(a_i^t, h_{gate_i}; \Theta_{ation}\right)\right) \qquad (20)$$

Where, δ_2 corresponds to the sigmoid activation function. Y_a and Y_h represents the linear transformations and $\chi, r_{\chi}$are the bias terms which forms a set of Θ_{ation} parameters, which characterizes the gate attention functions.

3.3 Feature extraction

Feature extraction refers to the process of transforming raw data into numerical features that can be processed while preserving the information in the original data set. It yields better results than applying machine learning directly to the raw data, where an object (also called segment) is a group of pixels with similar spectral, spatial or texture attributes. The traditional classification methods are pixel based, the spectral information in each pixel is used to classify and extract the images. Moreover, this paper is introduced with the integration of discrete wavelet transform, principle component analysis and gray level co-occurrence matrix for efficient feature extraction.

3.3.1 Discrete Wavelet Transform

The DWT [25] is an advanced technique of signal and image anslysis. It is developed as an alternative to short time Fourier, in order to overcome problems related to frequency and time resolution properties. Hence, the DWT of an image $a(e,l)\ of\ M \times M$ decomposition is determined by the equation (21).

$$a(e,l) = \sum_{f,i=0}^{M_j-1} v_{J,F,i}\varphi^{TT} J,F,i(e,l) + \sum_{R\in\mathbb{R}}\sum_{j=1}\sum_{f,i=0}^{M-1} y^R j,f,i\ \chi^R j,f,i(e,l) \qquad (21)$$

Here, this equation consists of various dilated functions and scaling functions. Therefore the DWT improves the extraction part of the proposed model.

3.3.2 Principle Component Analysis

Principal Component Analysis [26] is a mathematical technique to reduce the dimensionality of data. It works on the principal of factoring matrices to extract the principal pattern of a linear system. Hence, the principal component is determined in equation (22).

$$K_i = v_{i1}\, a_1^* + v_{i2}\, a_2^* + \ \ldots\ldots\ldots + v_{im}\, a_m^* \qquad (i = 1,2,\ldots,m) \qquad (22)$$

Where, a_i^* is the standardized indicator variable, which is represented by the equation (23).

$$a_i^* = (a_i - \bar{a_\iota})/e_i \qquad (23)$$

A comprehensive evaluation function of PCA is determined in equation (24)

$$K_{eval} = \frac{\xi_1}{\xi_1+\xi_2+\ldots+\xi_m} K_{eval_1} + \frac{\xi_2}{\xi_1+\xi_2+\ldots+\xi_m} K_{eval_2} + \ \ldots\ldots + \frac{\xi_m}{\xi_1+\xi_2+\ldots+\xi_m} K_{eval_m} \qquad (24)$$

Thus PCA plays an important role in determining the pattern of the image.

3.3.3 Gray Level Co-occurrence Matrix

GLCM [27] is a second-order statistical texture analysis method. It examines the spatial relationship among pixels and defines how frequently a combination of pixels are present in an image in a given direction and distance. The function to produce gray similarity level is defined in the equation (25).

$$GLCM_{level} = \sum_i \sum_j \frac{Q[i,j]}{1+|i-j|} \qquad (25)$$

Where, $[i,j]$ are the values in the row (i), column (j) and "Q"is the GLCM matrix.

3.4 Advanced Hybrid Extreme Learning Machine and Extreme Gradient Boosting

Image classification is the task of using computer vision and machine learning algorithms to extract meaning from an image, by assigning a label to an image from a predefined set of categories. In order to classify the oral cancer effectively, this paper proposes a machine learning model named as Advanced Hybrid Extreme Learning Machine and Extreme Gradient Boosting. AELm-XGB is a type of machine learning system that belongs to the supervised learning category. It is a single-layer feed forward neural network that randomly selects the input weights and analytically determines the output weights, which makes it scalable in the distributed gradient-boosted decision tree machine learning library. It also provides parallel tree boosting, which is the leading machine learning library for regression, classification, and ranking problems.

3.4.1 Advanced Hybrid Extreme Learning Machine

In the proposed method the AELm is an extreme learning machine [28], which is used as a classifier. This means that it does not need a learning process to calculate the parameters of the models, which remains constant during training and predicting phases. On the contrary, the weights that connect hidden nodes to outputs can be trained extremely fast. In this work, AELm is used for the classification of oral cancer based on the extracting texture features. The algorithm of AELm is given in Table 2.

Table 2: Algorithm for AELm computation

Advanced Hybrid Extreme Learning Machine Algorithm
Input: original features of the oral image $\psi_i i = 1, 2, \dots \dots$ Output: Classification of oral cancer Step 1: Initialize the parameters as in symbolic notation. $$e_{futs}(i) = \psi_i \quad and \quad i = 1, 2, 3, \dots \dots, m$$ $$\gamma_{-1} = 0 \; and \; \gamma_{-0} = 1$$ Step 2: For $f = 1 \; to \; t$ do $$bias_i \frac{x_{i-2} - 1}{x_{i-1}}$$ $$A_{fine}com^i = e_{futs}(i) + bias_i \left(e_{futs}(i) - e_{futs}(i-1)\right)$$ Step 3: Update the values of $e_{futs}(i+1)$. Step 4: Find the minimum value of regularization parameter L_{pram} among $\left(L_{pram_{i-1}}, 2L_{pram_{i-1}}, 3L_{pram_{i-1}}, \dots \dots \dots .\right)$ Step 5: $k\left(e_{futs}(i)\right) \leq h\left(L_{pram_i}, \; Vq^i\right) e_{futs}(i+1)$ Step 6: Substitute the L_{pram}values in AELm classifier Step 7: Evaluate minimum squared error rate (MSER) using, $$MIN_{SER} = \frac{i}{m}\sum_{i=1}^{m}\left(L_{pram_i} - \widetilde{L_{pram_i}}\right)^2$$ Step 8: If $MIN_{SER} \geq 0.1$ update $e_{futs}(i+1)$ value. Step 9: End For

Table 2 describes the AELm algorithm in which "ψ" represents the original features of oral image. $e_{futs}(i)$ determines the selected features of the oral image. L_{pram} denotes the regularization parameter. $A_{fine}com^i$ which is the affine combination of selected feature $e_{futs}(i)$ and $e_{futs}(i-1)$. Finally, MSER is calculated and its value is greater than or equal to 0.1 update the features of oral image. This iteration is repeated until features are selected for classification of oral image as healthy or cancerous.

3.4.2 Extreme Gradient Boosting

XG Boost [29] is a machine learning algorithm that belongs to the ensemble learning category, specifically the gradient boosting framework. It utilizes decision trees as base learners and employs regularization techniques to enhance model generalization. XG Boost is famous for its computational efficiency, offering efficient processing, insightful feature importance analysis, and seamless handling of missing values.

XGBoost can be used for classification, regression, and ranking problems. XG boosting is a type of gradient boosting (GB). GB is a boosting ensemble technique that makes predicators sequentially instead of individually. GB is a method that produces a strong classifier by combining weak classifiers. The goal of the GB, is building an iterative model that optimizes a loss function. It pinpoints the failings of weak learners by using gradients in the loss function to predict values, which is

determined in the equation (26).

$$W' = D(z) \quad (26)$$

The formula for minimizing loss function is depicted in equation (27).

$$MIN_{loss} = \frac{1}{m}\sum_i (w_i' - w_i)^2 \quad (27)$$

Now, the GB model with "N" phases and "n" as a message phase being $(1 \le n \le N)$, to improve the proposed model PRO_n a new estimator $g_n(z)$ is added. Therefore, the boosting equation is determined in equation (28).

$$g_n(z) = W - PRO_n(z) \quad (28)$$

Hence, XGBoost is better than other boosting algorithms, in terms of speed and performance. It is highly scalable and runs quicker as compared to the other traditional single machine learning algorithms. XGBoost handles the sparse data and implements several optimization and regularization techniques.

3.5 African Vulture Optimization

AVO [30] is a motivated optimization technique which is extensively used to solve several optimization problems in a wide range of fields. This is because, AVO outperforms other popular optimization algorithms in terms of execution time, convergence rate, and effectiveness. This optimization consists of five different stages, which is determined in Table 3 with its algorithm.

Table 3: Algorithm for African Vulture Optimization

African Vulture Optimization
Initial phase 1: Population grouping In this phase, following the formation of the initial population, the fitness of all solutions is determined, and the best solution is recognized, with the help of below equation. $$B(i) = \begin{cases} BEST_{vulre1} & if\ q_i = T_1 \\ BEST_{vulre1} & if\ q_i = T_2 \end{cases}$$ q_i calculation: $$q_i = \frac{B(i)}{\sum_{i=1}^{m} B(i)}$$ Phase 2: The Rate of Starvation of Vultures The exploration and exploitation stages of vultures may be constructed based on the behaviour. The K_i, a hunger level, of the i^{th} vulture at the l^{th}iteration is computed using the below equation. $$K_i = 2 \times RAN_i + 1 \times x \times 1 - \frac{ITER_i}{MAXITER} + l$$ Where, RAN_i and l is a random variable. The changes in the iteration determines the value of "l". $$l = g \times \left(sin^{y} \frac{\pi}{2} \times \frac{ITER_i}{MAXITER} + cos^{y} \frac{\pi}{2} \times \frac{ITER_i}{MAXITER} - 1 \right)$$ Phase 3: Exploration stage Vultures in the AVO can inspect various random locations using two distinct strategies. To choose one of the strategies during exploration phase, a random number RAN_{q_1} is used. $$Q_i + 1 = B_i - C_i \times K_i$$ Phase 4: Exploitation (First stage) The efficiency of AVO stage is explored. $$Q_i + 1 = \begin{matrix} C_i \times (K_i + RAN_i) - cl & if\ \ Q_2 \ge RAN_{q_2} \\ B_i - E_1 + E_2 & if\ \ Q_2 < RAN_{q_2} \end{matrix}$$ Phase 5: Exploitation (Second stage) The position can be updated in this phase. $$Q_i + 1 = \frac{X_1 + X_2}{2}$$ The effectiveness of AVO is increased by employing Levy Flight (LF) patterns. $$Levft_z = 0.001 \times \frac{v \times \delta}{u^{\frac{1}{\tau}}}$$ Finally, the best solutions are determined by AVO.

Therefore, the AVO is determined to lessen the error between the polarization profile of the estimated methods and the actual data extracted from the experimental data by optimizing it for finest results.

4. RESULTS AND DISCUSSION

The implementation of the proposed model is done using the python programming language and the system configuration is represented in the Table 3.

Table 3: System configuration

Component	Details
Platform	Anaconda (Spyder)
Processor	Intel(R) Core(TM) i5-3470 CPU @ 3.20GHz 3.20 GHz
System Type	64-bit operating system, x64-based processor
OS	Windows 10
RAM	8.00 GB

The hyperparameter used for proposed model is depicted in the Table 4.

Hyperparameter	Details
Conv.layers	9
Dense layers	4
Lambda layer	1
Activation function	Sigmoid, ReLU
Optimizer	Adam
Epochs	100
Learning rate	0.001
Loss	Binary

4.1 Datasets Description

The research utilizes the prominent real-time dataset. The dataset consists of 14,240 images for efficient oral detection. The label further represents normality and abnormality of the image. Hence, the mask images are obtained with the input images. The dataset images are divided for training and testing as 80% and 20% respectively.

4.2 Performance analysis and evaluation

The performance measures like accuracy, precision, recall, F1-score, ROC curve, Convergence curve, Computation time analysis, and the number of parameters will be calculated [31].The proposed models is evaluated for its effectiveness in segmentation phase in terms of Dice score, Intersection of Union and Hausdorff distance . The overall performance of proposed model in segmentation phase is represented in the Figure 4.

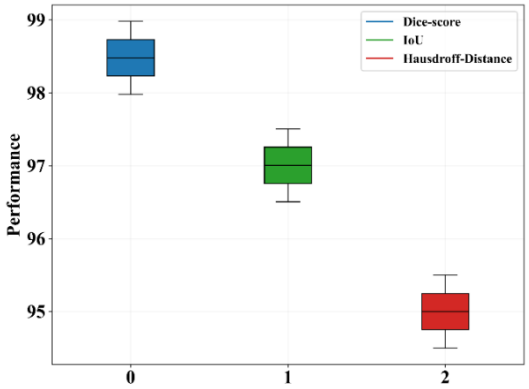

Figure 4: The overall performance of proposed ExpG-UNet model in segmentation phase

The proposed ExpG-UNet model provide high performance in the segmentation phase which is shown in the Figure 4. The evaluation of proposed model is made in terms of Dice score, IoU and Hausdorff distance and scored as 98.47, 97.0% and 95% respectively. This significant improvement demonstrates the proposed approach's superior ability to reliably in segmentation. It demonstrates the model's capacity to improve the reliability and effectiveness of cancer image analysis on the real-time dataset. The evaluation of ExpG-UNet in terms of accuracy is depicted in Figure 5.

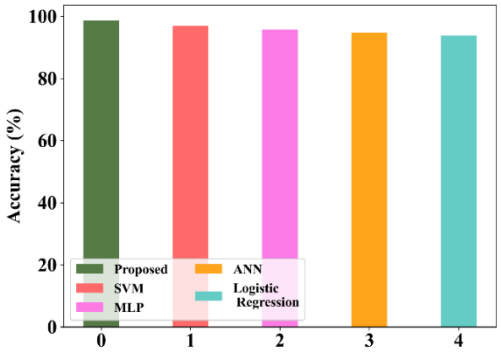

Figure 5: Accuracy analysis of proposed AElm-XGB model

The proposed AElm-XGB model provide notable accuracy which is shown in the Figure 5. The evaluation of proposed model is compared across various existing models like SVM, MLP, ANN, Logistic Regression, where the models reported an accuracy of 96.91%, 95.72%, 94.77% and 93.79% respectively. In contrast the proposed model outperforms with an accuracy of 98.67%. This notable accuracy highlights the performance of existing models in classification tasks. The evaluation of AElm-XGB in terms of recall is depicted in Figure 6.

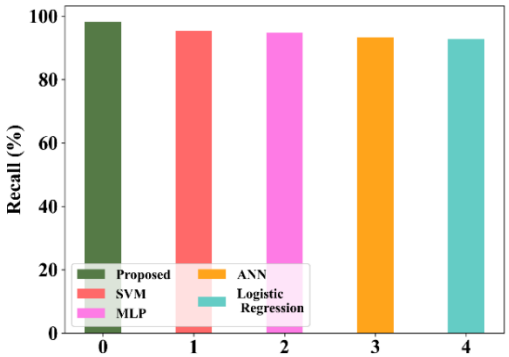

Figure 6: Comparative analysis of recall score of AElm-XGB model

The proposed AElm-XGB model provide a prominent recall score which is shown in the Figure 6. The evaluation of proposed model is compared across various existing models like SVM, MLP, ANN, Logistic Regression, where the models reported a recall score of 95.43%, 94.82%, 93.34% and 92.84% respectively. In contrast the proposed model outperforms with a recall score of 98.32%. This notable recall score highlights the performance of existing models in classification tasks. The evaluation of AElm-XGB in terms of precision is depicted in Figure 7.

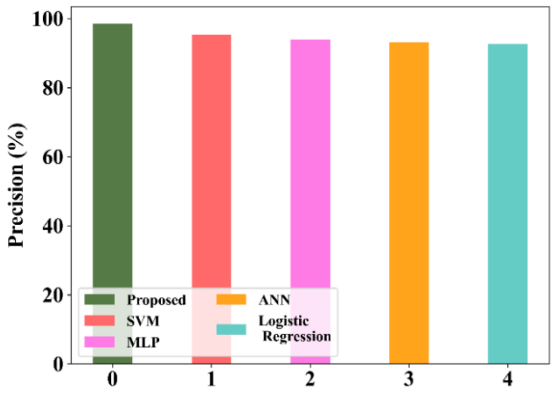

Figure 7: Precision score evaluation among existing models

The proposed AElm-XGB model provides a remarkable precision percentage which is shown in the Figure 7. The evaluation of proposed model is compared across various existing models like SVM, MLP, ANN, Logistic Regression, where the models reported a precision percentage of 95.41%, 94.03%, 93.19% and 92.77% respectively. In contrast the proposed model outperforms with a precision of 98.54%. The evaluation of AElm-XGB in terms of F1-score is depicted in Figure 8.

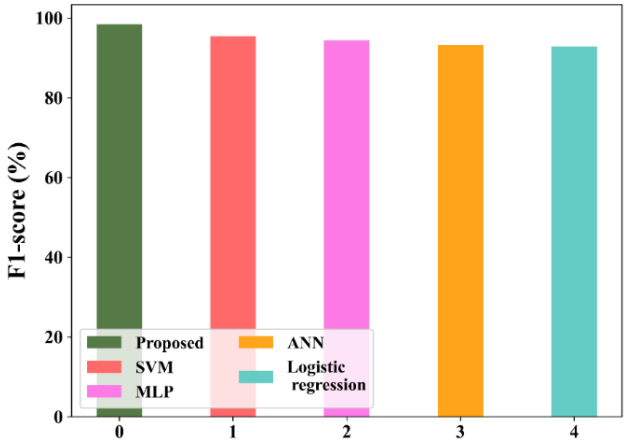

Figure 8: F1-score analysis of proposed AElm-XGB model

The proposed AElm-XGB model provides a remarkable F1-score which is shown in the Figure 8. The evaluation of proposed model is compared across various existing models like SVM, MLP, ANN, Logistic Regression, where the models reported with a F1-score of 95.42%, 94.42%, 93.27% and 92.80% respectively. In contrast the proposed model outperforms with a F1-score of 98.43%. The evaluation of AElm-XGB in terms of MSE is depicted in Figure 9.

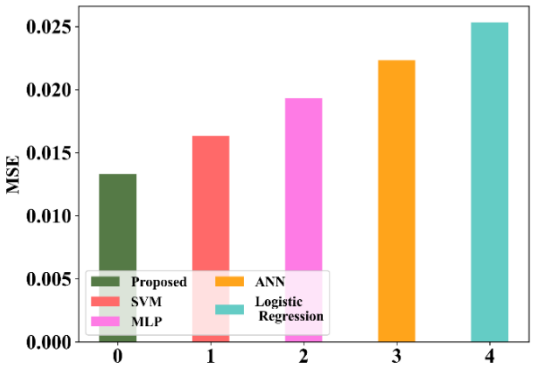

Figure 9: MSE score attained by AElm-XGB model and existing models

The proposed AElm-XGB model provides a significant MSE score which is shown in the Figure 9. The evaluation of proposed model is compared across various existing models like SVM, MLP, ANN, Logistic Regression, where the models reported with a MSE score of 0.016%, 0.019%, 0.022% and 0.025% respectively. In contrast the proposed model outperforms with a minimal MSE score of 0.013%. This underscores the AElm-XGB's enhanced performance. The evaluation of AElm-XGB in terms of RMSE is depicted in Figure 10.

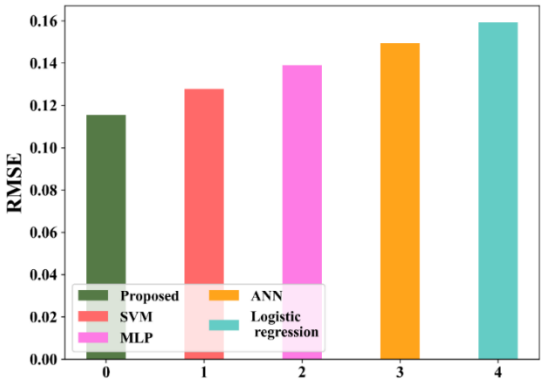

Figure 10: RMSE score attained by AElm-XGB model and existing models

The proposed AElm-XGB model provides a significant RMSE score which is shown in the Figure 10. The evaluation of proposed model is compared across various existing models like SVM, MLP, ANN, Logistic Regression, where the models reported with a RMSE score of 0.127%, 0.139%, 0.149% and 0.159% respectively. In contrast the proposed model outperforms with a minimal error score of 0.115%. This underscores the AElm-XGB's enhanced performance in reducing error. The evaluation of AElm-XGB in terms of MAE is depicted in Figure 11.

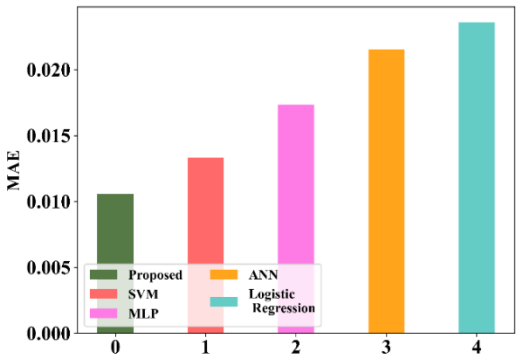

Figure 11: MAE score attained by AElm-XGB model and existing models

The proposed AElm-XGB model provides a substantial MAE score which is shown in the Figure 11. The evaluation of proposed model is compared across various existing models like SVM, MLP, ANN, Logistic Regression, where the models reported with a MAE score of 0.013%, 0.017%, 0.021% and 0.023% respectively. In contrast the proposed model outperforms with a minimal error score of 0.010%. The evaluation of AElm-XGB in terms of accuracy, loss in training and testing phases is depicted in Figure 12 (a) & (b).

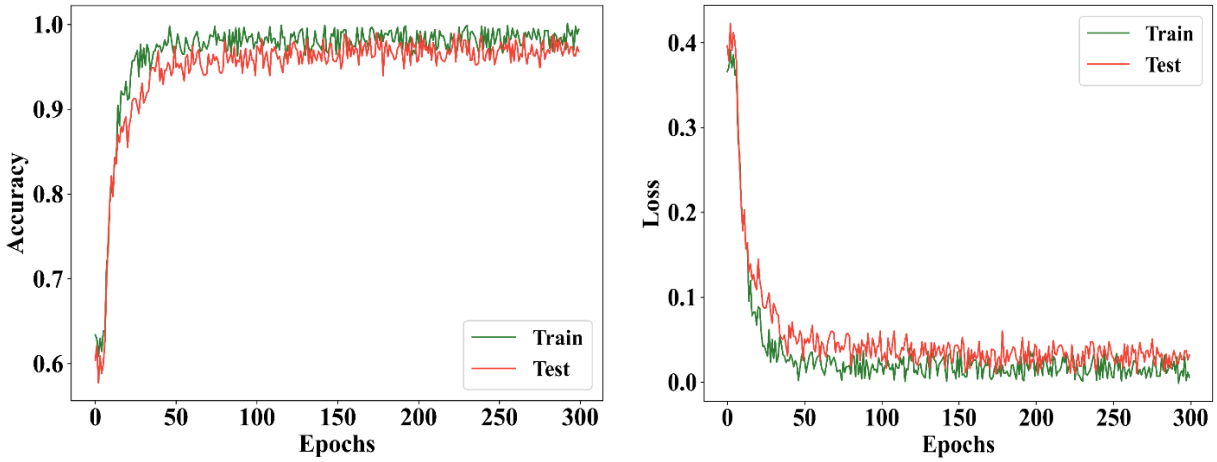

(a) (b)

Figure 12: Training and testing analysis (a) Accuracy (b) Loss

Figure 12 (a) determines the training and testing analysis of accuracy in which the x-axis represents the epoch size, ranging from 0 to 300, and the y-axis represents the accuracy, ranging from 0.6 to 1.0. The red line on the graph denotes the training accuracy, while the grey line represents the testing accuracy. The graph indicates a constant improvement in accuracy over the epochs, with a final accuracy of 98.67%. The high level of accuracy shows that the model is very good at learning the performance of the data. Figure 12 (b) determines the training and testing analysis of loss, in which the graph shows a continuous decrease in loss over the epochs, with both training and testing loss values. The graph for TPR across FPR is shown in figure 13.

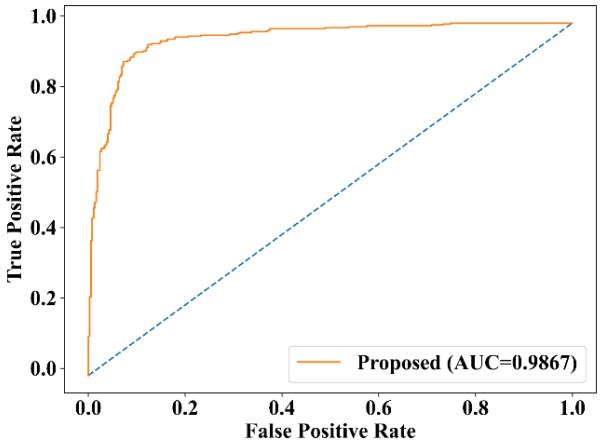

Figure 13: ROC analysis for proposed model

Figure 13 displays the performance evaluation of AElm-XGB, where the TPR is plotted against the FPR. The blue line represents the TPR as achieved by AElm-XGB, while the dotted line provides a comparative baseline performance. This graph effectively demonstrates the algorithm's capability in optimizing the trade-off between true positives and false positives, showcasing its efficiency in enhancing the model's accuracy. The evaluation of AElm-XGB in terms of convergence graph is depicted in Figure 14.

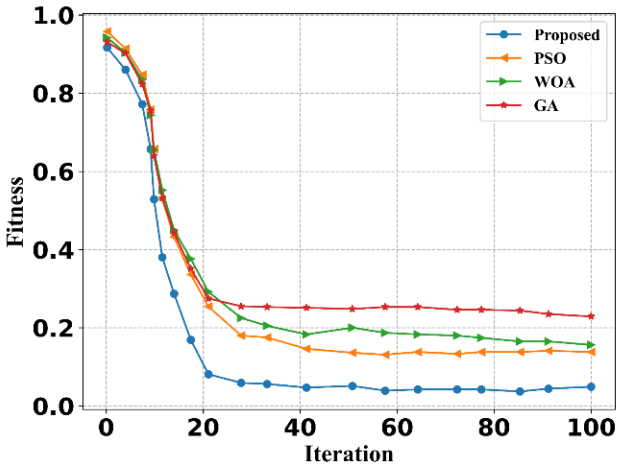

Figure 14: Convergence graph of AElm-XGB

Figure 14 displays the performance evaluation of AElm-XGB, where the fitness function is plotted against the Iterations. Here, the evaluation of proposed model is compared across various existing optimization techniques like PSO, WOA and GA. This convergence graph of AElm-XGB effectively demonstrates the algorithm's capability in optimizing the trade-off function between fitness and iteration, showcasing its efficiency in enhancing the model's correctness. The evaluation of AElm-XGB in terms of computational time is depicted in Figure 15.

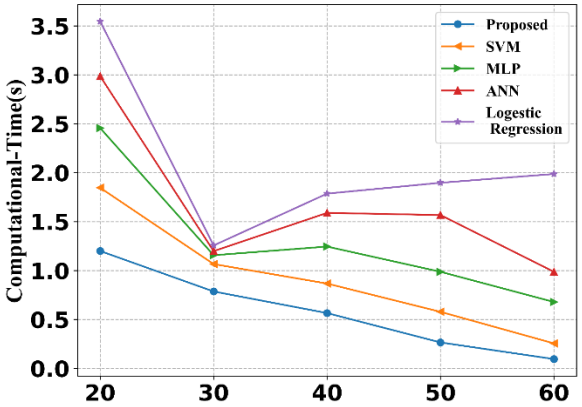

Figure 15: Computational time of AElm-XGB

The proposed AElm-XGB model provides a significant computational time, which is shown in the Figure 15. The evaluation of proposed model is compared across various existing models like SVM, MLP, ANN, Logistic Regression, where the models reported with a greater computational time of 30, 40, 50 and 60 respectively. In contrast the proposed model outperforms with a minimal computational time of 20. This underscores the AElm-XGB models enhanced performance. Finally, the ablation study of the proposed model is described in Table 5.

Table 5: Ablation study of the proposed model

Performance metric	Proposed	Without Pre-processing	Without segmentation	Without feature extraction	Without optimization
Accuracy	98.67%	96.52%	93.67%	89.76%	96.45%

Table 4 illustrates the ablation study of the proposed model in terms of accuracy. Initially without skipping any process the model achieves an outstanding accuracy of 98.67%. Which shows the enhanced performance of the model. Moreover,

without pre-processing there is a little decline with 96.52% accuracy. Further without segmentation and feature extraction there is a notable decline with an accuracy of 93.67% and 89.76%. Lastly without optimization the model poses a minimal decrease with an accuracy of 96.45%. Hence, it is essential to implement these process for effective computer vision tasks.

4.4 Discussion

In discussion, the proposed model demonstrates convincing advancements in oral cancer classification with effective segmentation. Kumari et al. [16], Jeyaraj et al. [17], Jubair et al. [18], Panigrahi et al. [19] and Huang et al. [20] lacked robust feature extraction, optimization techniques with poor and low quality images, which resulted in low accuracy. Using the AElm-XGB for classification and optimization, significantly enhances the oral cancer segmentation process. However, QCeHE increases the global contrast of the images. Further, the combination of DWT-PCA-GLCM performs effective extraction. Finally the model is boosted up by AVO optimization for reducing losses. Experimental results on real-time dataset demonstrates high accuracy, precision, recall and F1-score etc. These outcomes underscores the efficiency of the approach in stimulating active extraction and classification. Table 6 presents a comparative study of the performance of existing Models and the proposed AElm-XGB design.

Table 6: Correlative performance of existing methods with proposed method

Author & reference	Year	Model	Accuracy
Kumari et al. [16]	2023	SVM	80.95%
Jeyaraj et al. [17]	2019	CNN	91.4%
Jubair et al. [18]	2022	Light weight deep CNN	85.0%
Panigrahi et al. [19]	2022	Capsule Network	97.35%
Huang et al. [20]	2023	ISSA	97.33%
Proposed	2024	AElm-XGB	98.67%

Table 6 provides a comparison of performance between the proposed AElm-XGB model and several other adaptive designs. The proposed model demonstrates superior performance across accuracy when compared to the other models.

5. CONCLUSION

In conclusion, the proposed work AElm-XGB presents an innovative approach for OC classification using advanced machine learning techniques with innovative optimization systems. The method involves the utilization of the real-time datasets and the model is compared across various classification algorithms, including SVM, MLP, ANN and Logistic Regression. The proposed method demonstrated superior performance in all key metrics, achieving an accuracy of 98.67%, precision of 98.54%, recall of 98.32%, and 98.43% of F1 score. The integration of QCeHE, ApLG models further enhances the system's efficiency in processing and analyzing large datasets with effective noise removal. The DWT-PCA-GLCM models facilitated superior feature extraction and dimensionality reduction, contributing to the overall robustness and accuracy of the oral cancer detection. Moreover, the AElm-XGB classifies the oral cancer efficiently. The final optimization by AVO is done for optimum results. Further, the model also outperforms minimal MSE, RMSE and MAE with low computation time. Hence the results of this model confirm the viability of the proposed approach for enhancing OC segmentation with robust classification. Future work will focus on further refining the model for effective OC segmentation and exploring its applicability to other datasets and domains. Additionally, integrating this model with its capabilities to handle large-scale OC detectors will be key areas of development. Through continuous improvement and adaptation, this work aims to contribute significantly to the advancement of detection technologies.

REFERENCES

[1] López-Cortés, Xaviera A., Felipe Matamala, Bernardo Venegas, and César Rivera. "Machine-learning applications in oral cancer: a systematic review." Applied Sciences 12, no. 11 (2022): 5715.

[2] Rahman, Atta-ur, Abdullah Alqahtani, Nahier Aldhafferi, Muhammad Umar Nasir, Muhammad Farhan Khan, Muhammad Adnan Khan, and Amir Mosavi. "Histopathologic oral cancer prediction using oral squamous cell carcinoma biopsy empowered with transfer learning." Sensors 22, no. 10 (2022): 3833.

[3] Maryam, Siddra, Marcelo Saito Nogueira, Rekha Gautam, Shree Krishnamoorthy, Sanathana Konugolu Venkata Sekar, Kiang Wei Kho, Huihui Lu et al. "Label-Free Optical Spectroscopy for Early Detection of Oral Cancer." Diagnostics 12, no. 12 (2022): 2896.

[4] Al-Rawi, Natheer, Afrah Sultan, Batool Rajai, Haneen Shuaeeb, Mariam Alnajjar, Maryam Alketbi, Yara Mohammad, Shishir Ram Shetty, and Mubarak Ahmed Mashrah. "The effectiveness of artificial intelligence in detection of oral cancer." international dental journal 72, no. 4 (2022): 436-447.

[5] Al Duhayyim, Mesfer, Areej Malibari, Sami Dhahbi, Mohamed K. Nour, Isra Al-Turaiki, Marwa Ismael Obayya, and Abdullah Mohamed. "Sailfish Optimization with Deep Learning Based Oral Cancer Classification Model." Comput. Syst. Sci. Eng. 45, no. 1 (2023): 753-767.

[6] Chu, Chui S., Nikki P. Lee, John Adeoye, Peter Thomson, and Siu-Wai Choi. "Machine learning and treatment outcome prediction for oral cancer." Journal of Oral Pathology & Medicine 49, no. 10 (2020): 977-985.

[7] Das, Dev Kumar, Surajit Bose, Asok Kumar Maiti, Bhaskar Mitra, Gopeswar Mukherjee, and Pranab Kumar Dutta. "Automatic identification of clinically relevant regions from oral tissue histological images for oral squamous cell carcinoma diagnosis." Tissue and Cell 53 (2018): 111-119.

[8] Bur, Andrés M., Andrew Holcomb, Sara Goodwin, Janet Woodroof, Omar Karadaghy, Yelizaveta Shnayder, Kiran Kakarala, Jason Brant, and Matthew Shew. "Machine learning to predict occult nodal metastasis in early oral squamous cell carcinoma." Oral oncology 92 (2019): 20-25.

[9] D'souza, Sharon, and Veeranjaneyulu Addepalli. "Preventive measures in oral cancer: An overview." Biomedicine & Pharmacotherapy 107 (2018): 72-80.

[10] Lee, Tzu-Ying, and Yu-Hsin Tseng. "The potential of phytochemicals in oral cancer prevention and therapy: a review of the evidence." Biomolecules 10, no. 8 (2020): 1150.

[11] Abati, Silvio, Chiara Bramati, Stefano Bondi, Alessandra Lissoni, and Matteo Trimarchi. "Oral cancer and precancer: a narrative review on the relevance of early diagnosis." International journal of environmental research and public health 17, no. 24 (2020): 9160.

[12] Borse, Vivek, Aditya Narayan Konwar, and Pronamika Buragohain. "Oral cancer diagnosis and perspectives in India." Sensors International 1 (2020): 100046.

[13] Harsha, Choudhary, Kishore Banik, Hui Li Ang, Sosmitha Girisa, Rajesh Vikkurthi, Dey Parama, Varsha Rana et al. "Targeting AKT/mTOR in oral cancer: mechanisms and advances in clinical trials." International journal of molecular sciences 21, no. 9 (2020): 3285.

[14] Zhang, Qing, Dan Hou, Xueying Wen, Mengyu Xin, Ziling Li, Lihong Wu, and Janak L. Pathak. "Gold nanomaterials for oral cancer diagnosis and therapy: Advances, challenges, and prospects." Materials Today Bio 15 (2022): 100333.

[15] Jeyaraj, Pandia Rajan, Bijaya Ketan Panigrahi, and Edward Rajan Samuel Nadar. "Classifier feature fusion using deep learning model for non-invasive detection of oral cancer from hyperspectral image." IETE Journal of Research 68, no. 6 (2022): 4031-4042.

[16] Kumari, Alka, and Ashok Kumar Mehta. "The Effectiveness of Feature Extraction and Machine Learning based approach for Early Detection of Oral Cancer." (2023).

[17] Jeyaraj, Pandia Rajan, and Edward Rajan Samuel Nadar. "Computer-assisted medical image classification for early diagnosis of oral cancer employing deep learning algorithm." Journal of cancer research and clinical oncology 145 (2019): 829-837.

[18] Jubair, Fahed, Omar Al-karadsheh, Dimitrios Malamos, Samara Al Mahdi, Yusser Saad, and Yazan Hassona. "A novel lightweight deep convolutional neural network for early detection of oral cancer." Oral Diseases 28, no. 4 (2022): 1123-1130.

[19] Panigrahi, Santisudha, Jayshankar Das, and Tripti Swarnkar. "Capsule network based analysis of histopathological images of oral squamous cell carcinoma." Journal of King Saud University-Computer and Information Sciences 34, no. 7 (2022): 4546-4553.

[20] Huang, Qirui, Huan Ding, and Navid Razmjooy. "Optimal deep learning neural network using ISSA for diagnosing the oral cancer." Biomedical Signal Processing and Control 84 (2023): 104749.

[21] Acharya, Upendra Kumar, and Sandeep Kumar. "Image sub-division and quadruple clipped adaptive histogram equalization (ISQCAHE) for low exposure image enhancement." Multidimensional systems and signal processing 34, no. 1 (2023): 25-45.

[22] Hrytsyk, Volodymyr, Mykola Medykovskyy, and Mariia Nazarkevych. "Estimation of Symmetry in the Recognition System with Adaptive Application of Filters." Symmetry 14, no. 5 (2022): 903.

[23] Zhi, Yin-Cong, Yin Cheng Ng, and Xiaowen Dong. "Gaussian processes on graphs via spectral kernel learning." IEEE Transactions on Signal and Information Processing over Networks 9 (2023): 304-314.

[24] Huang, Hong, Panpan Liu, and Jie Liu. "TAGU-Net: Transformer Convolution Hybrid-Based U-Net With Attention Gate for Atypical Meningioma Segmentation." IEEE Access 11 (2023): 53207-53223.

[25] Zhao, Yawu, Shudong Wang, Yulin Zhang, Sibo Qiao, and Mufei Zhang. "WRANet: wavelet integrated residual attention U-Net network for medical image segmentation." Complex & intelligent systems 9, no. 6

(2023): 6971-6983.

[26] Usman, Tiwalade Modupe, Yakub Kayode Saheed, Djitog Ignace, and Augustine Nsang. "Diabetic retinopathy detection using principal component analysis multi-label feature extraction and classification." International Journal of Cognitive Computing in Engineering 4 (2023): 78-88.

[27] Scott, Isabelle, David Connell, Derek Moulton, Sarah Waters, Ana Namburete, Anurag Arnab, and Peter Malliaras. "An automated method for tendon image segmentation on ultrasound using grey-level co-occurrence matrix features and hidden Gaussian Markov random fields." Computers in Biology and Medicine 169 (2024): 107872.

[28] Priyadharshini, N., N. Selvanathan, B. Hemalatha, and C. Sureshkumar. "A novel hybrid Extreme Learning Machine and Teaching–Learning-Based Optimization algorithm for skin cancer detection." Healthcare Analytics 3 (2023): 100161.

[29] Maleki, Alireza, Mohammad Raahemi, and Hamid Nasiri. "Breast cancer diagnosis from histopathology images using deep neural network and XGBoost." Biomedical Signal Processing and Control 86 (2023): 105152.

[30] Shrivastava, A., Chakkaravarthy, M., Shah, M.A..A Novel Approach Using Learning Algorithm for Parkinson's Disease Detection with Handwritten Sketches. In Cybernetics and Systems, 2022

[31] Shrivastava, A., Chakkaravarthy, M., Shah, M.A., A new machine learning method for predicting systolic and diastolic blood pressure using clinical characteristics. In *Healthcare Analytics*, 2023, 4, 100219

[32] ST Siddiqui, H Khan, MI Alam, K Upreti, S Panwar, S Hundekari, A Systematic Review of the Future of Education in Perspective of Block Chain, Journal of Mobile Multimedia, 1221-1254

[33] Kamal Upreti, Anmol Kapoor, Sheela Hundekari,Deep Dive Into Diabetic Retinopathy Identification: A Deep Learning Approach with Blood Vessel Segmentation and Lesion Detection, 2024: Vol 20 Iss 2, https://doi.org/10.13052/jmm1550-4646.20210

[34] Ramesh Chandra Poonia; Kamal Upreti; Sheela Hundekari; Priyanka Dadhich; Khushboo Malik; Anmol Kapoor, An Improved Image Up-Scaling Technique using Optimize Filter and Iterative Gradient Method, 2023 3rd International Conference on Mobile Networks and Wireless Communications (ICMNWC) ,04-05 December 2023, 10.1109/ICMNWC60182.2023.10435962

[35] Venata Sai Chandra Prasanth Narisetty and Tejaswi Maddineni, Revolutionizing Mobility: The Latest Advancements in Autonomous Vehicle Technology, Nanotechnology Perceptions, 20 No. S12(2024),1354–1367.

[36] Venata Sai Chandra Prasanth Narisetty and Tejaswi Maddineni,Powering the Future: Innovations in Electric Vehicle Battery Recycling, Nanotechnology Perceptions 20 No. S13 (2024) 2338-2351.

[37] Prasad, Jayashree Rajesh, Rajesh Shardanand Prasad, Amol Dhumane, Nihar Ranjan, and Mubin Tamboli. "Gradient bald vulture optimization enabled multi-objective Unet++ with DCNN for prostate cancer segmentation and detection." Biomedical Signal Processing and Control 87 (2024): 105474.

[38] Zhu, Haihua, Zheng Cao, Luya Lian, Guanchen Ye, Honghao Gao, and Jian Wu. "CariesNet: a deep learning approach for segmentation of multi-stage caries lesion from oral panoramic X-ray image." Neural Computing and Applications (2023): 1-9.

[39] R. Sathya; V.C. Bharathi; S. Ananthi; T. Vijayakumar; Rvs Praveen; Dhivya Ramasamy, Real Time Prediction of Diabetes by using Artificial Intelligence, 2024 2nd International Conference on Self Sustainable Artificial Intelligence Systems (ICSSAS), DOI: 10.1109/ICSSAS64001.2024.10760985

[40] Rvs Praveen;B Vinoth;S. Sowmiya;K. Tharageswari;Purushothapatnapu Naga Venkata VamsiLala;R. Sathya, "Air Pollution Monitoring System using Machine Learning techniques for Smart cities," 2024 2nd International Conference on Self Sustainable Artificial Intelligence Systems (ICSSAS), DOI: 10.1109/ICSSAS64001.2024.10760948

[41] RVS Praveen;U Hemavathi;R. Sathya;A. Abubakkar Siddiq;M. Gokul Sanjay;S. Gowdish, "AI Powered Plant Identification and Plant Disease Classification System," 2024 4th International Conference on Sustainable Expert Systems (ICSES), DOI: 10.1109/ICSES63445.2024.10763167

[42] Neeraj Kumar;Sanjay Laxmanrao Kurkute;V. Kalpana;Anand Karuppannan;RVS Praveen;Soumya Mishra, "Modelling and Evaluation of Li-ion Battery Performance Based on the Electric Vehicle Tiled Tests using Kalman Filter-GBDT Approach" 2024 International Conference on Intelligent Algorithms for Computational Intelligence Systems (IACIS), DOI: 10.1109/IACIS61494.2024.10721979